Micromachined Ultrasonic Transducers (MUTs)

I. Ladabaum, B. T. Khuri-Yakub, D. Spoliansky*, M. I. Haller**

E. L. Ginzton Laboratory, Stanford University, Stanford, CA 94305
*Ecole Normale Supérieure, Paris, France
**Acuson, Mountain View, CA

Abstract --- The fabrication and modeling of ultrasonic air transducers is reported. The transducers are made using surface micromachining techniques, which enable the realization of capacitive transducers with center frequencies ranging from 1 MHz to 12 MHz. Transmission experiments in air at 3.1 MHz, 5.6 MHz, 9.2 MHz, and 11.4 MHz are reported. Custom circuitry is able to detect capacitance fluctuations on the order of 10^{-18} F and fluctuating as fast as 20 MHz. The transducers can be optimized for either transmission or reception. By leveraging the precise structural control provided by micromachining, receivers with displacement sensitivity well in the sub-angstrom range can be fabricated. Such detection sensitivity is shown to yield transducer systems with a 100 dB signal to noise ratio. An improved theoretical model for the transducers is presented. The theoretical model describes the static behavior of the membrane. Theoretical predictions of the dynamic behavior of the membrane also agree well with experimental results.

INTRODUCTION

The generation of ultrasound in air is challenging because the acoustic impedance of air (400 kg/m^2s) is many orders of magnitude smaller than the impedance of piezoelectric materials commonly used to excite ultrasonic vibrations (~$30x10^6$ kg/m^2s). The large impedance mismatch implies that piezoelectric air transducers are inherently inefficient. In order to improve efficiency, a matching layer is usually placed in between the piezoelectric and the air. The matching layer solution is problematic for three reasons. First, the impedance mismatch is so large that matching layer materials with the necessary characteristic impedance are rarely available. Second, the improved energy coupling comes at the expense of bandwidth. Third, high frequency transducers require impractically thin matching layers. Attempts to maximize the energy transfer from the piezoelectric element to the air and vice versa have achieved moderate success[1-3]. However, the increased complexity of the more efficient devices reduces their reliability and increases their cost.

Transducers based on electrostatic actuation offer more promise than optimized piezoelectric transducers. Although magnetoacoustic and capacitive devices have been reported [4-8], our transducer system is the first to demonstrate 11.4 MHz transmission in air. Furthermore, we present a simplified theoretical model which accounts for the behavior observed.

DEVICE FABRICATION AND OPERATION

The MUT consists of circular silicon nitride membranes suspended above heavily doped silicon bulk (Figure 1). When a voltage is applied between the membrane and the bulk, electrostatic forces attract the membrane toward the bulk and stress forces within the membrane resist the attraction. If the membrane is driven by an alternating voltage at its mechanical resonance frequency, large displacements, and consequently significant sound generation, will result. Conversely, if the membrane is biased appropriately and subjected to ultrasonic waves at resonant frequencies, significant detection currents will be generated. Micromachining is the chosen vehicle for device fabrication because the membrane's dimensions (microns) and residual stress (hundreds of MPa's) can be tailored to yield mechanical resonance frequencies in the MHz range. Silicon and silicon nitride have excellent mechanical properties, and can be readily patterned using the wide repertoire of procedures invented by the semiconductor industry.

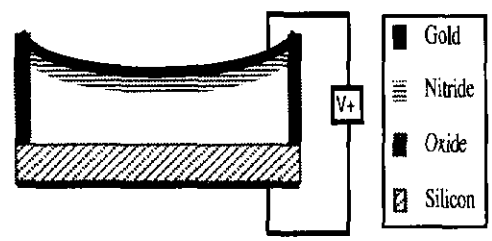

Figure 1: Schematic of one element of a MUT.

The fabrication sequence is simple (Figure 2). A highly doped, p-type <100> 4" silicon wafer is cleaned and a 1μm oxide layer is grown with a wet oxidation process. A 5000 Å layer of LPCVD nitride is then

0-7803-2940-6/95/$4.00

deposited. The residual stress of the nitride can be varied by changing the proportion of silane to ammonia during the deposition process. After the backside of the wafer is stripped, a chrome adhesion layer and a 500 Å film of gold are evaporated onto both sides of the wafer. A pattern of etchant holes is then transferred to the wafer lithographically, followed by a gold and nitride etch. Thus, access holes are generated through which HF can subsequently attack the sacrificial oxide layer. The etch time determines the dimensions of the membrane. One transducer consists of a matrix of individual elements with a spacing of 25, 50 or 100 μm.

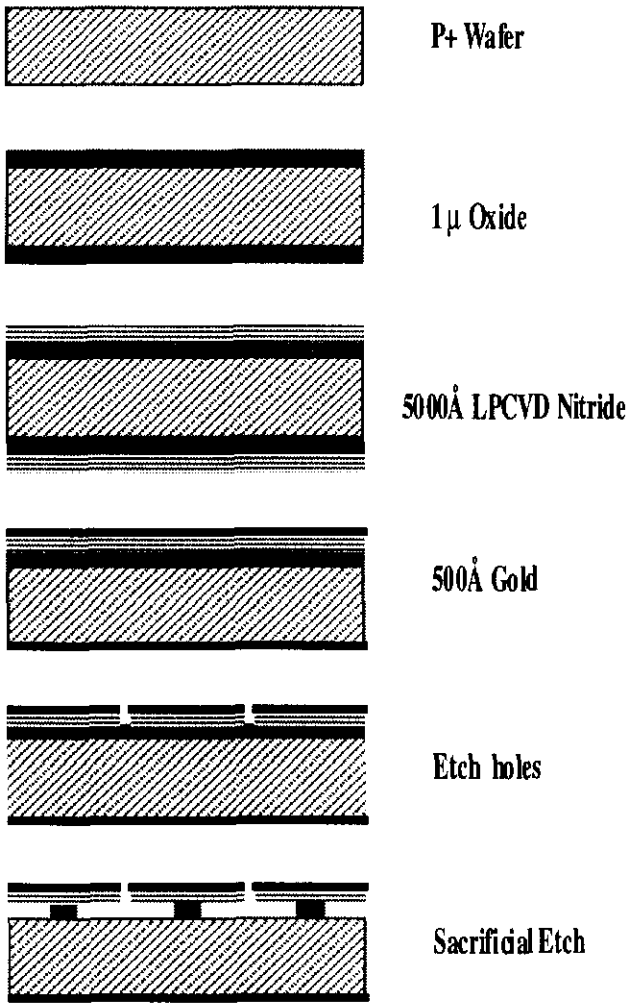

Figure 2: Fabrication sequence

The theoretical model accounts for both the static and dynamic behavior of the device. The static analysis allows an understanding of the operating point about which the dynamic analysis applies. Because the electrostatic attraction force varies as the square of the electrode separation, while the restoring force varies approximately linearly, certain voltages and separations lead to membrane collapse. Furthermore, the behavior is hysteretic; after collapse, the membrane requires a fairly low voltage condition to snap back (Figure 3).

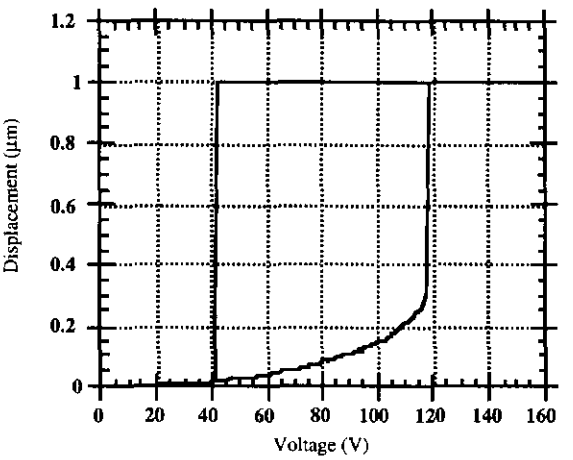

Figure 3: Collapse and hysteretic behavior of membrane.

The static analysis begins with the general plate equation[9]:

$$\frac{(Y_0 + A\sigma)t_m^3}{12(1-\upsilon^2)}\nabla^4 x - \sigma t_m \nabla^2 x - P_E(r) = 0 \qquad (1)$$

where Y_0 is Young's modulus, A is area, σ is residual stress, t_m is the membrane thickness, υ is Poisson's ratio, x is membrane displacement, and $P_E(r)$ is the electrostatic pressure as a function of radius. Neglecting bending stresses and introducing polar coordinates yields the membrane equation:

$$\sigma t_m\left(\frac{d^2x}{dr^2} + \frac{1}{r}\frac{dx}{dr}\right) + P_E(r) = 0 \qquad (2)$$

The Green function for this equation is:

$$G(r,\xi) = \begin{cases} \xi \ln(\xi) \rightarrow 0 < \dfrac{r}{a} < \xi < 1 \\ \xi \ln\left(\dfrac{r}{a}\right) \rightarrow 0 < \xi < \dfrac{r}{a} < 1 \end{cases} \qquad (3)$$

where a is the membrane radius and ξ is a variable of integration. The solution for the displacement as a function of radius then becomes:

$$\frac{a^2}{\sigma t_m}\int_0^1 G(r,\xi)P_E(\xi)d\xi \qquad (4)$$

which we solve iteratively on a computer.

The dynamic analysis begins by adding the membrane's inertia term to (2):

$$\sigma t_m\left(\frac{d^2x}{dr^2}+\frac{1}{r}\frac{dx}{dr}\right)+\rho t_m\frac{d^2x}{dr^2}+P_E(r)=0 \qquad (5)$$

where ρ is the membrane density. The solution, when taking $P_E(r)=P_{uniform}$ and using phasor analysis, is found to be:

$$x(r)=\frac{P_{uniform}}{\omega^2\rho t_m}\left[\frac{J_0(kr)}{J_0(ka)}-1\right] \qquad (6)$$

where ω is frequency $k=\omega\sqrt{\rho/\sigma}$ and J_0 is the zeroth order Bessel function. If we define the mechanical impedance of the membrane as the ratio of pressure to average velocity, we obtain:

$$Z_m=\frac{P_{uniform}}{v_{average}}=\frac{-i\omega\rho t_m kaJ_0(ka)}{\left[2J_1(ka)-kaJ_0(ka)\right]}A \qquad (7)$$

Equation (7) can be used to derive a two-port model[9]. Computer simulations using the two-port model match the experimental results of transmission, in air at 9.2 MHz (Figure 4). Transmission experiments at 11.4MHz, 5.6 MHz and 3.1 MHz show similar agreement.

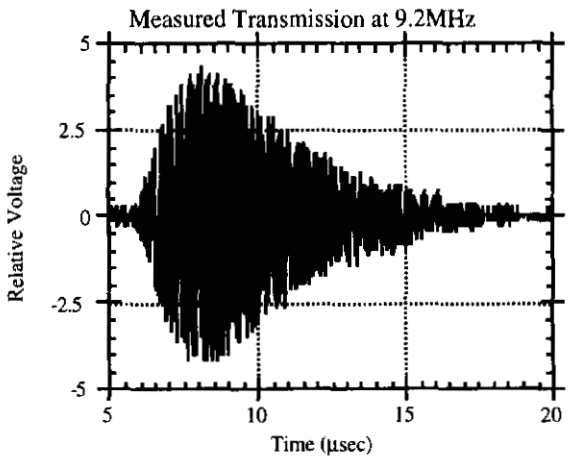

Figure 4a: Transmission at 9.2 MHz: Experiment

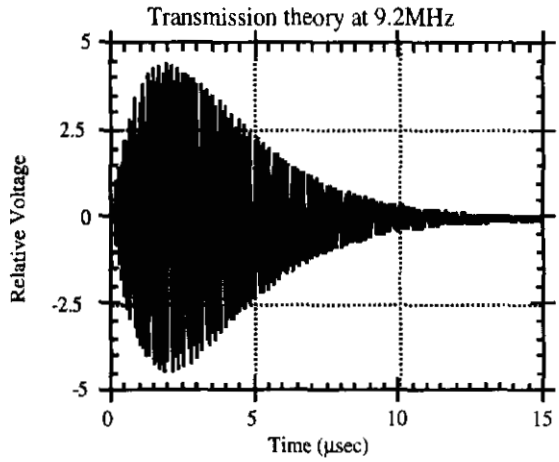

Figure 4b: Transmission at 9.2 MHz: Theory

The transmission experiments necessitated the development of transducer packaging, a custom 6 degrees of freedom tilt stage, and custom detection circuitry. The custom detection circuitry consists of a transconductance amplifier system used to detect the currents generated by the transducer. The first generation circuitry had some bugs which restricted the experiments to less than 0.5 cm of transducer separation. The devices, when properly connected, are sensitive enough to withstand the severe attenuation of ultrasound in hair, however, and we await the completion of the amplifier to perform a second round of experiments.

A first order analysis yields:

$$I=d\frac{(CV)}{dt}$$

which, in phasor form with constant voltage, becomes:

$$I=\omega VC$$

For our circuit, the noise floor is 20pA/Hz$^{1/2}$ as per a circuit simulator. For a 10 MHz transducer with a 2 MHz bandwidth operating at a 60 V bias, the noise floor corresponds to a capacitance of 7.5×10^{-18} F. Thus, a 100 pF transducer with a 1 m gap can detect displacements on the order of 10^{-3} Å. The fundamental noise floor of a MUT, however, is set by the thermal motion of the membrane. The air surrounding the membrane buffets it into motion, as do the thermal vibrations of the solid parts of the MUT. The noise can be calculated using the real part of the transducer's impedance (Figure 5)[10]. The same 100 pF MUT of above thermally vibrates 0.003Å RMS. A 0.3 m emitter coupled with a 0.003Å receiver results in a system with 120dB of dynamic range. It is thus clear that these transducers are capable of high power excitation and high sensitivity detection, enabling many applications requiring a large dynamic range.

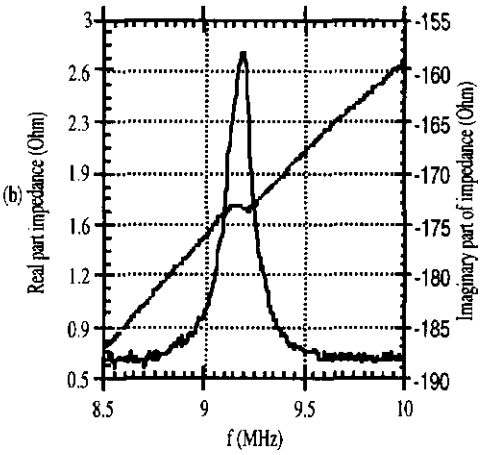

Figure 5: Impedance spectrum of 9.2 MHz device

The bandwidth of the devices is determined by the final shape of each resonant element. For transducers made from independent circular elements, the bandwidth is of the order of 5%. For transducers in which an element's etching results in membrane continuity with its neighbors, the bandwidth is measured to be of the order of 20%. Ultra-high bandwidth can be achieved through a judicious distribution of individual elements with varying center frequencies. Thus, high efficiency and broad bandwidth can be achieved.

CONCLUSION

In summary, we have reported the transmission of high frequency ultrasound in air. We have described the technology and the theory that govern the behavior of the transducers used in the transmission experiments. We showed that broad band transducer systems capable of withstanding 100 dB of loss are feasible, an accomplishment that has significant implications in the fields of imaging and nondestructive evaluation.

ACKNOWLEDGMENT

We would like to acknowledge the support of ONR.

REFERENCES

[1] L. C. Lynnworth, IEEE Trans. Son. Ultrason. SU **12,** 37 (1965).
[2] S. Schiller, C. K. Hsieh, C. H. Chou, and B.T. Khuri-Yakub, Rev. Prog. Quant. NonDestr. Eval. **9**, 795 (1990).
[3] M. I. Haller and B.T. Khuri-Yakub, Proc. IEEE Ultrason. Symp. 937 (1992)
[4] C. Edwards and S. B. Palmer, IEEE Trans. on Mag. **26**, 2080 (1990).
[5] G. M. Sessler, Sensors and Actuators A (Physical) **A26**, 323 (1991).
[6] W. Kuhnel and G. Hess, Sensors and Actuators A (Physical) **A32**, 560 (1992).
[7] D. W. Schindel, D. A. Hutchins, IEEE Trans. Ultrason., Ferroelect., Freq. Cont. **42**, 42 (1995).
[8] M.I. Haller, *Micromachined Ultrasonic Devices and Materials*, Doctorate Thesis, (Stanford University, 1994).
[9] W. P. Mason, *Electromechanical Transducers and Wave Filters* (Van Nostrand,New York, 1942).
[10]T.B. Gabrielson, IEEE Trans. Elect. Dev. **40**, 903 (1993)